Eur. J. Biochem. 206, 705–719 (1992)

Multi-frequency EPR and high-resolution Mössbauer spectroscopy of a putative [6Fe-6S] prismane-cluster-containing protein from *Desulfovibrio vulgaris* (Hildenborough)

Characterization of a supercluster and superspin model protein

Antonio J. PIERIK[1], Wilfred R. HAGEN[1], W. Richard DUNHAM[2] and Richard H. SANDS[2]

[1] Department of Biochemistry, Agricultural University, Wageningen, The Netherlands
[2] Biophysics Research Division, Institute of Science and Technology, The University of Michigan, Ann Arbor, USA

(Received January 27, 1992) – EJB 92 0100

The putative [6Fe-6S] prismane cluster in the 6-Fe/S-containing protein from *Desulfovibrio vulgaris*, strain Hildenborough, has been enriched to 80% in ^{57}Fe, and has been characterized in detail by S-, X-, P- and Q-band EPR spectroscopy, parallel-mode EPR spectroscopy and high-resolution ^{57}Fe Mössbauer spectroscopy. In EPR-monitored redox-equilibrium titrations, the cluster is found to be capable of three one-electron transitions with midpoint potentials at pH 7.5 of +285, +5 and −165 mV. As the fully reduced protein is assumed to carry the $[6Fe\text{-}6S]^{3+}$ cluster, by spectroscopic analogy to prismane model compounds, four valency states are identified in the titration experiments: $[6Fe\text{-}6S]^{3+}$, $[6Fe\text{-}6S]^{4+}$, $[6Fe\text{-}6S]^{5+}$, $[6Fe\text{-}6S]^{6+}$. The fully oxidized 6+ state appears to be diamagnetic at low temperature. The prismane protein is aerobically isolated predominantly in the one-electron-reduced 5+ state. In this intermediate state, the cluster exists in two magnetic forms: 10% is low-spin $S = 1/2$; the remainder has an unusually high spin $S = 9/2$. The $S = 1/2$ EPR spectrum is significantly broadened by ligand (2.3 mT) and ^{57}Fe (3.0 mT) hyperfine interaction, consistent with a delocalization of the unpaired electron over 6Fe and indicative of at least some nitrogen ligation. At 35 GHz, the g tensor is determined as 1.971, 1.951 and 1.898. EPR signals from the $S = 9/2$ multiplet have their maximal amplitude at a temperature of 12 K due to the axial zero-field splitting being negative, $D \approx -0.86\ cm^{-1}$. Effective $g = 15.3$, 5.75, 5.65 and 5.23 are observed, consistent with a rhombicity of $|E/D| = 0.061$. A second component has $g = 9.7$, 8.1 and 6.65 and $|E/D| = 0.108$. When the protein is reduced to the 4+ intermediate state, the cluster is silent in normal-mode EPR. An asymmetric feature with effective $g \approx 16$ is observed in parallel-mode EPR from an integer spin system with, presumably, $S = 4$. The fully reduced 3+ state consists of a mixture of two $S = 1/2$ ground state. The g tensor of the major component is 2.010, 1.825 and 1.32; the minor component has $g = 1.941$ and 1.79, with the third value undetermined. The sharp line at $g = 2.010$ exhibits significant convoluted hyperfine broadening from ligands (2.1 mT) and from ^{57}Fe (4.6 mT). Zero-field high-temperature Mössbauer spectra of the protein, isolated in the 5+ state, quantitatively account for the 0.8 fractional enrichment in ^{57}Fe, as determined with inductively coupled plasma mass spectrometry. The six irons are not equivalent; the six quadrupole pairs are in a 2:1 pattern. Upon reduction to the 3+ state, the spectra change shape dramatically with indication of localized valencies. Four of the six irons appear to be relatively unaffected, while the remaining two exhibit a considerable increase in quadrupole splitting and an increase in the isomer shift, each consistent with a full charge reduction. From temperature and field-dependent Mössbauer studies on the 5+ and 3+ states, it is concluded that all six irons are paramagnetic and part of the same spin system. A mixed-ligand prismane model is proposed in which four Fe form an electron-delocalized core, flanked on opposite sites by two Fe of distinctly more ionic character, as they are coordinated by nitrogen. In the corresponding vector-coupling model for the $S = 9/2$ state, the two ionic ferric ions couple ferromagnetically through the delocalized core structure. With the characterization of this model protein, a frame of reference is provided for the spectroscopic study of more complex Fe/S enzymes.

Correspondence to W. R. Hagen, Laboratorium voor Biochemie, Landbouwuniversiteit, Dreijenlaan 3, NL-6703 HA Wageningen, The Netherlands

Abbreviation. ICP-MS, inductively coupled plasma mass spectrometry.

Enzymes. Desulfoviridin, dissimilatory sulfite reductase (EC 1.8.99.1); carbon-monoxide dehydrogenase, acetyl-CoA synthase (EC 1.2.99.2); nitrogenase (EC 1.18.6.1); Fe-hydrogenase (EC 1.18.99.1).

Over the past few years, we have tried to gain insight into the nature of the Fe/S cluster(s) of complex redox enzymes, namely, Fe-hydrogenase [1–3], MoFe-nitrogenase [4, 5], sulfite reductase [6] and carbon-monoxide dehydrogenase [7, 8]. These enzymes appear to have two general properties in common. They all exhibit unusual EPR spectra that have, in several instances, been identified as resulting from a very high

cluster spin $S = 7/2$ and $S = 9/2$. Also, the number of iron and acid-labile sulfur ions associated with the clusters appears to be significantly higher than the maximum of 4Fe/S encountered in other proteins. Hence, we use the terms superspin and supercluster as epithets for this type of cluster [9].

The enzymes just mentioned all contain a considerable number of Fe and acid-labile S^{2-} grouped into several clusters. This complexity, combined with the lack of structural information on these proteins, makes the study of their clusters presently difficult. In an attempt to tackle this problem from a different perspective a model protein, the prismane protein from *Desulfovibrio vulgaris* has been studied. The purification and biochemical characterization of this 6Fe/S-containing protein is described in [10]. We have previously presented EPR spectroscopic evidence indicating that the 6Fe/S are arranged in a single [6Fe-6S] supercluster [11]. We describe below an EPR and Mössbauer spectroscopic analysis of the prismane protein in different redox states. The combined results allow us to propose a structural model and a magnetic-coupling model for the biological 6Fe cluster.

MATERIALS AND METHODS

The purification and biochemical characterization of the prismane protein from *D. vulgaris* (subspecies Hildenborough), NCIB 8303, is described in [10].

Metallic iron 95.2% enriched in ^{57}Fe was obtained from Russia via Intersales-Holland BV, Hengelo, NL. The growth of *D. vulgaris* on ^{57}Fe-enriched medium in a 240-l batch culture differed from the standard procedure only in that tap water was replaced with demineralized water, and the iron source in the growth medium was replaced with ^{57}Fe-EDTA (255 mg metallic iron). Precultures were also grown on enriched medium. Enrichment of the batch culture was estimated to be $\leq 87\%$ based on colorimetric Fe determinations of the concentrated growth medium before and after addition of ^{57}Fe-EDTA stock. A determination of the $^{57}Fe/^{56}Fe$ ratio in the total concentrated growth medium with inductively coupled plasma/mass spectrometry (ICP-MS, courtesy of Drs C. Hess-Riechmann and K. Schneider, Universität Bielefeld, FRG) gave an enrichment of $77 \pm 3\%$. The final enrichment after growth and purification was $78 \pm 3\%$, as determined with ICP-MS on a sample of purified [3] desulfoviridin. This corresponds with the value of 80% as determined by quantitative Mössbauer spectroscopy (see Results and Discussion).

Deuterium oxide, 99.8 ^2H atoms/100 H atoms, and 30% (by mass) sodium deuteroxide in ^2H_2O (>99 ^2H atoms/100 H atoms), both from Janssen Chimica (Beerse, Belgium), were used to prepare deuterated Hepes buffer, p^2H 7.5. Prismane protein in ^2H_2O was prepared by diluting purified protein 1:40 in deuterated Hepes buffer and reconcentration on a Centricon YM30 device. This procedure was repeated once. The final global enrichment was checked with ^1H NMR to be 99 ^2H atoms/100 H atoms).

Reductive titrations were done at 25 °C in a 1.5-ml anaerobic cell under purified argon. The bulk potential of the stirred solution was measured at a Radiometer P-1312 platinum microelectrode with respect to the potential of a Radiometer K-401 saturated calomel electrode. Reported potentials are all recalculated with reference to the normal hydrogen electrode. The freshly prepared reductant and oxidant were sodium dithionite and $K_3Fe(CN)_6$ in 0.5 M anaerobic Hepes, pH 7.5. Redox equilibrium was obtained as judged by the attainment of a stable solution potential within a few minutes after addition of the titrant to the reaction mixture. The enzyme solution in 50 mM Hepes, pH 7.5, was incubated with the following mixture of mediators (each at a final concentration of 40 μM): *N,N,N′,N′*-tetramethyl-*p*-phenylenediamine; 2,6-dichloroindophenol; phenazine ethosulfate; methylene blue; resorufine; indigo disulfonate; 2-hydroxy-1,4-naphthoquinone, anthraquinone disulfonate, phenosafranine; safranine O; neutral red; benzyl viologen; methyl viologen. At equilibrium samples were drawn and transferred to EPR tubes under a slight overpressure of purified argon, then directly frozen in liquid nitrogen.

Normal-mode X-band EPR data were taken in Wageningen on a Bruker 200 D EPR spectrometer with peripheral instrumentation and data acquisition/quantification as described before [6]. Effective g values for $S = 9/2$ spectra were calculated as previously outlined [4, 6]. Parallel-mode X-band EPR was measured in the laboratory of Dr. S. P. J. Albracht (The University of Amsterdam) on a Varian E-9 EPR spectrometer equipped with the Varian E-236 bimodal rectangular cavity, as previously described in [12]. The spectrometer in Amsterdam was also used for Q-band measurements using Albracht's helium-flow system for the 35-GHz cylindrical cavity [13]. Additional X-band data and all the S-band and P-band data were collected in Ann Arbor on a Varian E-112 spectrometer and on the home-built S-band and P-band spectrometers described in [14]. The microwave source in the S-band spectrometer is a 70-mW solid-state oscillator; the P-band spectrometer has a 200-mW klystron. In all four frequency bands, the modulation frequency was 100 kHz.

Mössbauer spectra were obtained with a home-built spectrometer and associated hardware as described elsewhere [15, 16]. Part of the spectra presented have been corrected for source line shape and converted from transmission to absorption spectra. Previous examples of this approach to Mössbauer spectroscopy of ^{57}Fe-proteins, including theoretical simulation of experimental spectra, can be found in [17, 18].

RESULTS AND DISCUSSION

EPR of the 3+ state in dithionite-reduced protein

Throughout the paper we will label redox states as 3+, 4+, 5+ and 6+. This labeling is based on the assumption that the fully reduced prismane protein contains a $[6Fe\text{-}6S]^{3+}$ cluster. The reader is reminded that this is a working hypothesis based on three previous observations [11]: (a) the Fe stoichiometry is approximately six; (b) there is a striking similarity in g values between model compounds containing the $[6Fe\text{-}6S]^{3+}$ core and dithionite-reduced prismane protein; (c) the EPR signal of the dithionite-reduced protein integrates to approximately one $S = 1/2$ system/protein molecule.

We have assumed that both the prismane models and the dithionite-reduced prismane protein have magnetically isolated $S = 1/2$ ground states. The assignment of $S = 1/2$ to the models is consistent with magnetic susceptibility data and with the temperature and frequency dependence of the EPR [19]. An EPR line-width study of one of the prismane models indicated that magnetic isolation was only marginally achievable by trading off EPR signal/noise for chemical, therefore magnetic, dilution (cf. Fig. 7 in [19]). This problem of line broadening is typical of the EPR of small model compounds in frozen solution; however, it is generally absent from

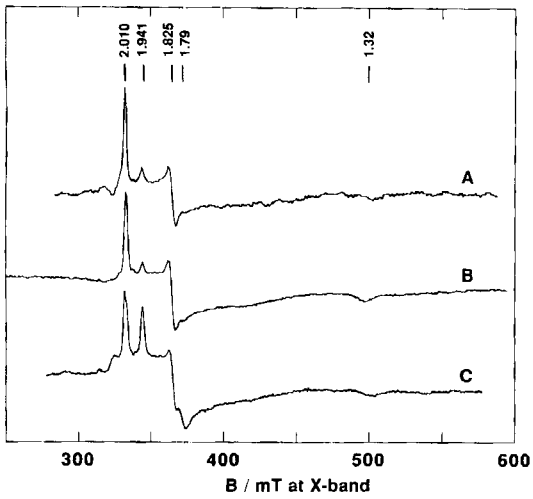

Fig. 1. Prismane-fingerprint EPR from the dithionite-reduced *D. vulgaris* (Hildenborough) prismane protein (the 3+ state). (A) P-band spectrum of 0.35 mM protein in 50 mM Hepes buffer, pH 7.5; (B) X-band spectrum of the same sample to show that the g values are frequency independent; (C) X-band spectrum of a different sample showing an increased ratio of the minor over the major component. EPR conditions: microwave frequency, 15484, 9224, 9337 MHz; microwave power, 40, 200, 200 mW; modulation amplitude, 0.4, 1, 0.8 mT; temperature, 15 K.

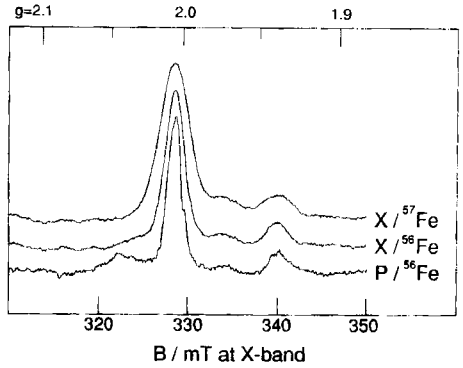

Fig. 2. Hyperfine (^{57}Fe), superhyperfine (^{14}N), and g-strain broadening of the $g = 2.010$ line from dithionite-reduced prismane protein. The data analysis is explained in the text. EPR conditions are as in Fig. 1.

metalloprotein EPR, where the protein serves as a natural diamagnetic diluant [20].

We are thus in a better position with the prismane protein to look for signs of interaction in the EPR. In our initial analysis of the X-band spectrum, we already noted extra features in addition to the expected three g turning points [11]. With reference to Fig. 1 B, we note that the most striking of these features is the extra absorption peak at $g = 1.941$ between the highest two g values, 2.010 and 1.825; other features are found between the lowest two g values, 1.825 and 1.32, and as low-field and high-field shoulders. Note that the g values 2.010 and 1.825, reported here, are a slight correction (i.e. +0.005) to the previously reported values [11]. However, these values are also measured from the spectral turning points and not based on any rigorous mathematical analysis of the spectral shape.

For EPR studies, we have made 12 preparations of prismane protein each from a separate 240-l batch culture. Each sample exhibited the typical pattern of Fig. 1 B, although the relative intensities of the intermediate features compared to the main g peaks appeared to vary slightly. In only one out of the 12 preparations, the intermediate peak at $g = 1.941$ has a considerably increased intensity compared to the $g = 2.010$ peak, although the purification procedure was standard. A spectrum from this single sample is given in Fig. 1 C, as it indicates that the $g = 1.941$ peak is a separate spectral entity with a second g at 1.79. The third g is undetermined.

Following the early work on prismane models [19], the prismane protein was also subjected to multi-frequency EPR at 3–35 GHz. Just as with the models, it was found that samples of prismane protein gave detectable signals in X- and P-bands and not in S- and Q-bands. The P-band spectrometer is special in that it takes regular-sized X-band samples and with these reaches the sensitivity of the X-band machines. In Fig. 1 A and B, we compare the 15-GHz and 9-GHz spectrum. All features appear to be independent of frequency. Specifically, the two sets of g values 2.010, 1.825 and 1.32, and 1.941 and 1.79, are real g tensors. However, the low-field shoulder and the very broad feature around $g_{\text{eff}} \approx 1.6$ are also unaffected. Thus, the spectrum is not standard in that there are more frequency-invariant features than g tensor components. The shape of the spectrum from the 3+ state (specifically, the intensity ratio of the $g = 2.010$ and $g = 1.941$ species) is independent of the pH when measured in 0.2 M Mes, pH 5.5, or 0.2 M Ches, pH 9.5 (not shown).

Hyperfine broadening of the 3+ state EPR

Contributions from unresolved hyperfine components to the spectrum are presented in Fig. 2. As the frequency independence of peak positions implied electron spin-spin interactions to be insignificant, the line shape is taken to be a Gaussian from a convolution of g-strain and hyperfine broadening [20]. Since the different broadening mechanisms are physically independent, we have for the overall inhomogeneous line width:

$$W = \sqrt{(W^2_{g\text{-strain}} + W^2_{\text{metal hyperfine}} + W^2_{\text{ligand hyperfine}})}\,, \quad (1)$$

where the last term is the sum broadening of all independent contributions from all nuclear magnetic ligands. The second term is only significantly non-zero for ^{57}Fe-enriched protein. When measured in magnetic-field units, the first term changes linearly with the microwave frequency; the other two terms are frequency independent. Thus, the three spectra in Fig. 2 form a sufficient data set to determine the individual three components of W along the g-tensor z-axis. The observed full width at half height for the three spectra at $g = 2.010$ (from top to bottom) are 3.95, 2.61 and 3.11 mT, which yields

$W_{g\text{-strain}} = 1.2(5)$ mT at X-band (9225 MHz),

$W_{\text{metal hyperfine}} = 2.9(6)$ mT (frequency independent),

$W_{\text{ligand hyperfine}} = 2.2(9)$ mT (frequency independent).

Given a set of n equivalent nuclei, where the enrichment factor of an $I = 1/2$ nucleus has the average value f, we can write the probability of the combination where exactly i of the n nuclei have $I = 1/2$ as

$$f^i(1-f)^{n-i}\binom{n}{i}, \quad (2)$$

where $\binom{n}{i}$ is the binominal coefficient and represents the number of permutations of the combination. Referring to previous

work on hyperfine patterns [21], the Fourier transform of the entire pattern in the present case is

$$\sum_{i=0}^{n} f^i (1-f)^{n-i} \binom{n}{i} \cos^i(At/2)\,, \qquad (3)$$

where t is the argument of the Fourier space and A is the hyperfine constant. By back-transforming test spectra from the above equation, we were able to establish that

$$A_{Fe} = g\, W_{\text{metal hyperfine}}/5.0\,, \qquad (4)$$

if $n = 6$, W (mT) is the full width at half height, and f equals 0.8 (80% enrichment, as determined by ICP-MS and by Mössbauer quantitation). Therefore, 'A_z' (^{57}Fe) $\approx$ 1.2 mT, where the quotation marks are to indicate that we measure along the z-axis of the g tensor. This number is similar to the 'A_z' values for iron hyperfine splittings in the [4Fe-4S]$^{3+}$, [2Fe-2S]$^{1+}$ and [4Fe-4S]$^{1+}$ clusters in proteins as determined by EPR and electron nuclear double resonance [22–24].

The most striking contribution to the linewidth is the 2.29 mT from unresolved ligand hyperfine splittings. This number is much too high to be caused only by magnetic nuclei (H, N) in the second and/or higher coordination spheres. The corresponding number at g_z for [2Fe-2S]$^{1+}$ in spinach ferredoxin can be calculated from Fig. 4 in [25] to be approximately 1 mT. Thus, in the prismane protein there is some 2 mT additional broadening. We take this to indicate that the protein ligation to the prismane is not exclusively through cysteine sulfur, but also involves nitrogen.

The peak at $g = 2.010$ was also studied at X-band with a sample in deuterated buffer. No sharpening was detectable compared to the spectrum of Fig. 2 (not shown). Therefore, exchangeable protons do not contribute to the line width.

Multi-frequency $S = 1/2$ EPR of the 5+ state

We previously reported a signal from the prismane protein as it was isolated [11]. Temperature dependence indicated the signal to represent an $S = 1/2$ system; however, quantitation amounted to only 0.1 spin/protein molecule. The signal is unusual for an iron-sulfur protein in that all three g values are below the free-electron value. The g values and substoichiometric intensity are typical for d^1 ions such as Mo(V) or W(V); however, in preliminary analytical determinations, we were unable to detect these elements in the protein. We proposed that the signal is from [6Fe-6S]$^{5+}$ (*ibidem*; see also below). In more extensive elemental analyses, the content of Mo and W has now been determined to be <0.03/protein molecule (cf. [10]). We have now further characterized the signal by multi-frequency EPR.

In Fig. 3, the $g<2$ spectrum of the isolated protein is presented at four different microwave frequencies, 3–35 GHz. Evidently, the signal is from a single g tensor ($S = 1/2$) as three features are observed whose position on a g-value scale does not depend on the frequency. Unusual for iron-sulfur EPR, g anisotropy is virtually completely blurred in the inhomogeneous line shape at S-band. This broadening from unresolved ligand hyperfine splittings is considerable even at X-band. Only at the Q-band frequency hyperfine broadening has become insignificant compared to g-strain broadening, and we can rather accurately read out the g-tensor principal elements as 1.971, 1.951 and 1.898.

In Fig. 4, the X-band and P-band traces of Fig. 3 are replotted as dotted traces to compare them to the spectra from prismane protein enriched in ^{57}Fe. We decompose contributions to the line width along the same lines as for the 3+ spectra in Fig. 2. However, here we look at the peak at the lowest g value, $g = 1.898$, as the low-field part of the spectrum has insufficient resolution. The observed line-width values are 3.75 mT and 5.86 mT (^{57}Fe) in P-band and 2.80 mT and 3.75 mT (^{57}Fe) in X-band. From these numbers we obtain:

$$W_{\text{g-strain}} = 1.8 \text{ mT at X-band (9227 MHz)}\,,$$

$$W_{\text{metal hyperfine}} = 4.6 \text{ mT (frequency independent)}\,,$$

$$W_{\text{ligand hyperfine}} = 2.1 \text{ mT (frequency independent)}\,.$$

The value for $W_{\text{metal hyperfine}}$ is the average of the numbers obtained from the P-band (4.50 mT) and X-band (4.83 mT) spectra.

Again using the Fourier transform of the hyperfine pattern, we now find that A_x (^{57}Fe) $\approx$ 1.7 mT. This is somewhat

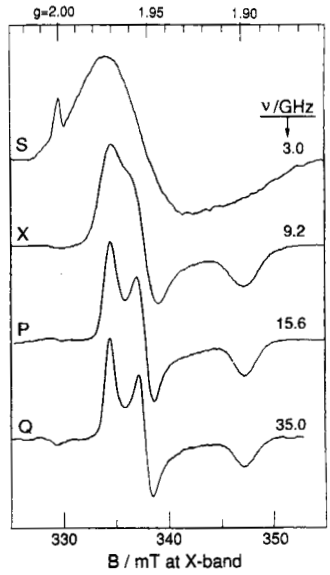

Fig. 3. Frequency dependent $S = 1/2$ EPR from the isolated prismane protein (the 5+ state). The data reveal a single g tensor plus an unusually large contribution of ligand hyperfine broadening. EPR conditions (S, X, P, Q): microwave frequency, 2966, 9225, 15557, 35018 MHz; microwave power, 0.44, 0.5, 5, 126 mW; modulation amplitude, 0.16, 1, 0.4, 1.25 mT; temperature, 19, 15, 15, 20 K.

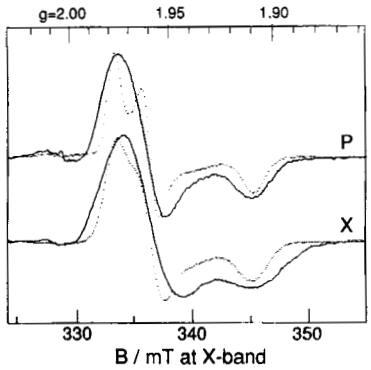

Fig. 4. Hyperfine (^{57}Fe), superhyperfine (^{14}N), and g-strain broadening of the $S = 1/2$ signal from the isolated prismane protein. Samples 80% enriched in ^{57}Fe. The data analysis is explained in the text. EPR conditions are as in Fig. 3.

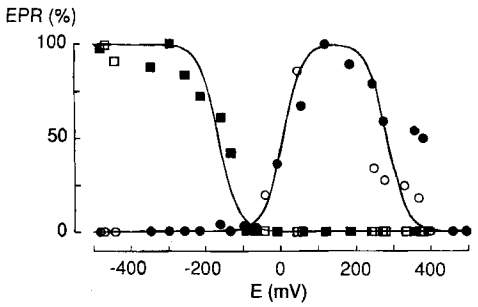

Fig. 5. Oxido-reductive titration at pH 7.5 of $S = 1/2$ components in *D. vulgaris* prismane protein with dithionite and ferricyanide in the presence of mediators. (□, ■) The prismane-fingerprint signal (the 3+ state) monitored at $g = 1.825$; (○, ●) signal with all $g < 2$ (the 5+ state) monitored at $g = 1.898$. (■, ●) Titration in two directions starting from the isolated protein, which corresponds approximately to the top of the bell-shaped curve. (□, ○) A titration starting from the fully pre-oxidized state. EPR conditions: microwave frequency, 9.33 GHz; microwave power, 13 mW; modulation amplitude, 0.63 mT; temperature, 15 K.

higher than that found for the 3+ state and, thus, also somewhat higher than the value common for regular Fe/S clusters. Note that the $[6Fe\text{-}6S]^{3+}$ is isoelectronic with $3[2Fe\text{-}2S]^{1+}$ (average Fe valency of +2.5), however, the $[6Fe\text{-}6S]^{5+}$ structure has no analog in simple Fe/S (bio)chemistry. The increased Fe hyperfine interaction is not the result of the electron spin being less delocalized onto the protein ligand, because the magnitude of the ligand hyperfine broadening is comparable to that in the 3+ state. This latter observation is another indication of nitrogen coordination to the cluster.

Again, as with the 3+ spectrum, deuteration of the buffer did not result in a sharper X-band spectrum (not shown).

Redox titrations monitored with $S = 1/2$ EPR

The prismane protein was anaerobically titrated with reductant and oxidant in the presence of a mixture of redox mediators covering a broad potential range (see Materials and Methods). The result of these titrations in 50 mM Hepes, pH 7.5, is presented in Fig. 5 as relative EPR intensities of the $S = 1/2$ signals assigned above to the 3+ and the 5+ state. The isolated protein is in an intermediate redox state, the 5+ state, and this still holds after mixing with the mediator cocktail. Thus, the starting point of the titration, before addition of titrant, has an equilibrium potential of some +100 mV vs the normal hydrogen electrode. From this point, the protein was reductively titrated with sodium dithionite and oxidatively titrated with potassium ferricyanide. In a second experiment (the open symbols in Fig. 5), reversibility was tested as follows: the protein was first completely oxidized with ferricyanide to the EPR silent 6+ state, then it was partially re-reduced with dithionite to the 5+ state, and finally it was stepwise reduced with dithionite to full reduction or re-oxidized with ferricyanide to the 6+ state. The solid lines in Fig. 5 are $n = 1$ Nernst curves.

The titration clearly defines four separate redox states corresponding to the putative valencies 3+ to 6+ of the [6Fe-6S] cluster. The $S = 1/2$ prismane signal of the 3+ state, detected at $g_z = 1.825$, appears with a midpoint potential of −165 mV. We have previously shown that this signal represents approximately 0.6−0.9 spin/50-kDa protein molecule [11]. With the corrected molecular mass of 52 kDa [10], and including the spin intensity of the minor component with $g_z = 1.941$ (single-integration method), the complete EPR spectrum of reduced protein essentially represents unit stoichiometry, therefore, the percentage reduction on the ordinate axis is an absolute value.

The titration of the $S = 1/2$ signal with all $g < g_e$ ascribed to the 5+ state has the typical bell shape of an intermediate redox state. We previously found a spin intensity of 0.10−0.12 in the isolated enzyme [11]. The plateau of the bell-shaped curve in Fig. 5 also corresponds to some 0.1 spin/protein molecule. The isolated protein is indeed predominantly in the 5+ state. This conclusion implies that we should account for the missing 90% intensity of this half-integer spin system (see below).

The 5+ signal disappears upon reduction with dithionite as an $n = 1$ acceptor with a midpoint potential of −5 mV. The cluster comes into the 4+state which should be integer spin or $S = 0$. Consistent with this assignment, no signal is observed in regular-mode EPR.

When the 5+ state is oxidized with ferricyanide, we also expect to make an even-electron system. Indeed, we observe the 5+ signal to disappear with no new signals detected. Apparently, the 6+ state is diamagnetic, $S = 0$. In this capacity to reach reversibly the fully oxidized state, the putative [6Fe-6S] cluster differs from the classical dinuclear and cubane clusters. We observe some hysteresis in the oxidation curve that is probably not intrinsic to the protein. In the potential range around +0.3 V, where appropriate mediators are not available, it is difficult to establish redox equilibrium. The $n = 1$ Nernst fit on all points gives a 6+/5+ potential of +285 mV; however, it should be obvious that this number is significantly less accurate than the other two reduction potentials.

Characterization of an $S = 9/2$ system from the 5+ state

In the 5+ state, only 10% of the protein is recovered in the $S = 1/2$ spectrum. If the concept of a cluster in a single valence state is valid then the remaining 90% should also be half-integer spin. We have, therefore, looked for high-spin EPR in concentrated samples of the prismane protein.

The isolated protein has a number of weak resonances at low magnetic field values. The temperature dependence of these lines can be seen in Fig. 6. For the non-saturated spectrum of a ground-state Kramers doublet, the signal amplitude should decrease with increasing temperature. It is clear from Fig. 6 that the amplitudes of the high-spin resonances go through a maximum as a function of temperature. Therefore, these resonances are from one or more excited states. The spectrum has its maximal amplitude at a temperature of about 12 K. We use this spectrum (Fig. 7) for a g analysis.

The spectral feature with the lowest magnetic field value has an absorption shape peaking at an effective g of 15.3. This observation is the starting point for our analysis that develops along the same lines as our recent identification of $S = 9/2$ EPR in *D. vulgaris* dissimilatory sulfite reductase [6]. We take the system spin to be half-integer and the relevant spin Hamiltonian to be

$$H_s = D[S_z^2 - S(S+1)/3] + E(S_x^2 - S_y^2) + g\beta B \cdot S . \quad (5)$$

We assume, as is very common for metalloprotein EPR, that the Zeeman interaction is considerably smaller than the zero-field interaction, i.e. we are in the weak-field limit. This assumption is tested later by estimating the magnitude of the

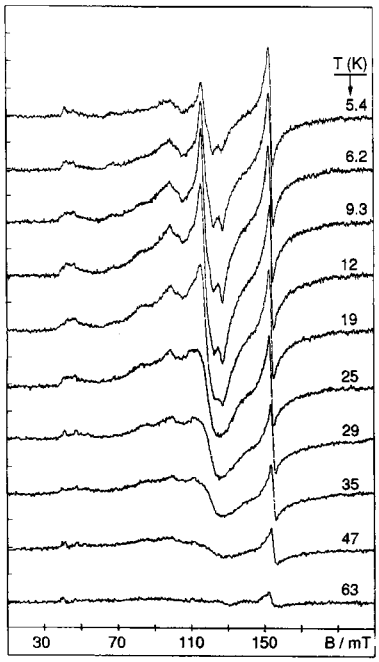

Fig. 6. Temperature dependence of low-field $S = 9/2$ resonances from *D. vulgaris* prismane protein in the 5+ state. For all spectra, spectrometer settings were the same except for temperature. The line at $g = 4.3$ (155 mT) is from adventitious ferric ion and is partially saturated at low temperatures. The other signals are not saturated. EPR conditions: microwave frequency, 9.33 GHz; microwave power, 80 mW; modulation amplitude, 0.8 mT.

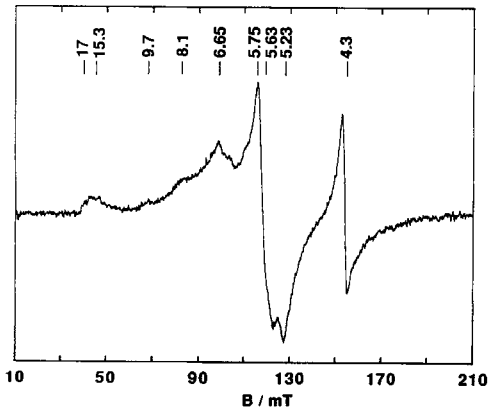

Fig. 7. Effective g assignment of the low-field $S = 9/2$ EPR. The spectrum was recorded at the optimal temperature of 12 K, i.e. at which the amplitude is maximal and lifetime broadening is not significant. EPR conditions were as in Fig. 6.

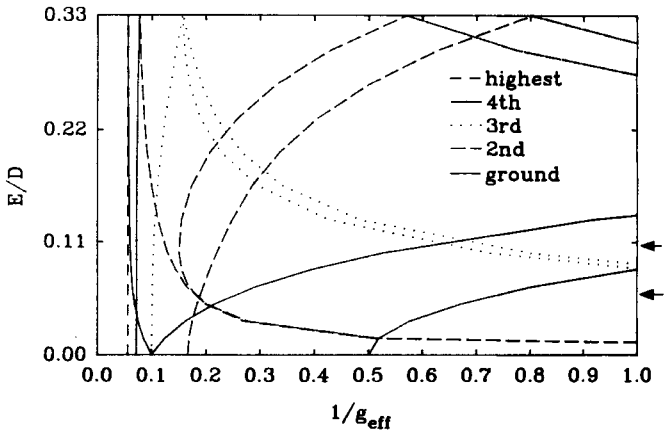

Fig. 8. Rhombogram (inverted representation) for $S = 9/2$ calculated in the weak-field limit (i.e. $D > g\beta B$) with real $g = 2.00$. The present form of the rhombogram is an alternative to the linear representation (cf. [6]) and allows for a direct read-out of all peak positions for a given rhombicity, E/D, on a reciprocal effective g scale, i.e. on a linear magnetic-field scale. The two arrows indicate the two rhombicities found for the prismane protein $S = 9/2$ EPR (cf. Fig. 7 and Table 1).

zero-field splitting parameter, D. Under these assumptions, and with the real value, $g \approx 2$, the system spin S and the highest effective g are related as $4S \geq g_{max}$. We observe that $g_{eff} = 15.3$, therefore, the system spin is $S \geq 9/2$. As in [6], we assume $S = 9/2$ and we proceed to prove consistency with the observed (Fig. 7) effective g values.

In the weak-field limit, and with the real g fixed at 2.00, the five times three effective g of the EPR subspectra from within the Kramers doublets of the $S = 9/2$ system are a function of the rhombicity, $0 \leq |3E/D| \leq 1$, only. We have recently given a graphic representation (the rhombogram) of these relations for $S = 9/2$ in [6]. An alternative, fully analogous representation (the inverted rhombogram) is obtained by plotting the rhombicity against the inverse of the effective g values, as in Fig. 8. Fitting of the experimental g values comes down to moving a horizontal line along the rhombicity axis of Fig. 8, where the intersections of this line with all curves define a stick spectrum of effective g values on an inverse g scale, i.e. on a linear magnetic-field scale.

The peak at $g = 15.3$ can only come from the $|\pm 1/2>$ doublet. Since its amplitude goes through a maximum with increasing temperature, the zero-field splitting parameter, D, must be negative. The $|\pm 1/2>$ doublet has the highest energy within the $S = 9/2$ multiplet. The $g = 15.3$ line defines a rhombicity of $E/D = 0.061$ and this value in turn defines all the other 14 g values (Table 1). The second g of the $|\pm 1/2>$ doublet is predicted at $g = 3.8$. However, with an inhomogeneous broadening from isotropic g strain (cf. [20]), the line width should be $(15.3/3.8)^2$ approximately 16 times greater than that at $g = 15.3$. Evidently, this line is not observable. The main prediction for $E/D = 0.061$ is a near-isotropic, therefore easily observable, spectrum from within the $|\pm 3/2>$ doublet at $g = 5.2-5.7$. This is indeed the major feature of the spectrum in Fig. 7.

The other features of Fig. 7 are not fit by the model. The line at $g = 4.3$ is of course the well-known isotropic resonance from contaminating ferric ion ($S = 5/2$, $|E/D| \approx 1/3$, $m_s = \pm 3/2$). The remaining resonances at $g = 9.7$, 8.1 and 6.65 fit the $S = 9/2$ model for $E/D = 0.108$, and $m_s = \pm 3/2, \pm 5/2$. The $S = 9/2$ spin occurs in two forms of different rhombicities. This is a very common phenomenon in high-spin EPR of metalloproteins. It was also observed for the $S = 9/2$ system in sulfite reductase [6]. The relative intensities of the two sets of lines varies slightly from preparation to preparation (not shown). The rhombicity $E/D = 0.108$ predicts a line at $g = 16.7$ for the $|\pm 1/2>$ doublet. With equal probability for the two rhombicities, the amplitude of this peak should be about 20% of that at $g = 15.3$ as a consequence of the increased g anisotropy. We observe sufficient intensity at $g = 16.7$ to account for this prediction.

Table 1. Calculated and observed effective g-values for $S = 9/2$ in *D. vulgaris* (Hildenborough) prismane protein in the 5+ state. The theoretical g values were calculated in the weak-field limit as in [6]. The following abbreviations are used: wide, too wide to be detected; outside, resonance line falls outside range of magnetic field; obsc, obscured by adventitious iron signal; n.s., no significant transition probability.

E/D	Doublet	g_z	g_y	g_x
0.061	$\|\pm1/2>$	1.32 wide	15.25 15.3	3.78 wide
	$\|\pm3/2>$	5.23 5.2(3)	5.74 5.7(5)	5.68 5.6(5)
	$\|\pm5/2>$	9.89 9.7	0.47 outside	0.55 outside
	$\|\pm7/2>$	13.98 n.s.	≈0 outside	≈0 outside
	$\|\pm9/2>$	18.00 n.s.	≈0 outside	≈0 outside
0.108	$\|\pm1/2>$	0.73 wide	16.66 17	1.66 wide
	$\|\pm3/2>$	4.42 obsc	8.06 8.1	6.68 6.6(5)
	$\|\pm5/2>$	9.62 9.7	1.44 wide	1.61 wide
	$\|\pm7/2>$	13.92 n.s.	≈0 outside	≈0 outside
	$\|\pm9/2>$	17.98 n.s.	≈0 outside	≈0 outside

Temperature dependence and quantification of the $S = 9/2$ EPR

The magnitude of the zero-field splitting can be obtained from a fit of EPR intensity to a Boltzmann distribution over the $S = 9/2$ multiplet. The close-to-isotropic pattern around $g \approx 5.5$ from within the $|\pm3/2>$ doublet is the subspectrum with the largest amplitude. The feature with the next-to-highest intensity is the derivative line at $g = 6.65$. We have used both the area of the $g \approx 5.5$ feature and the amplitude of the positive lobe at $g \approx 6.7$ with respect to the base line at zero-field as the $|\pm3/2>$ intensity to fit the Boltzmann distribution over the five doublets as a function of the temperature. The results are graphically presented in the Fig. 9B. Both fits are optimal for $D = -0.86\ \text{cm}^{-1}$. This result is not significantly sensitive to whether we calculate the energy levels for axial symmetry ($E = 0$) or for the intermediate rhombic case with $|E/D| = 0.1$. We have also taken the first integral of the feature peaking at $g = 15.3$ as the $|\pm1/2>$ intensity, and the corresponding fit gives essentially the same value of $D = -0.86\ \text{cm}^{-1}$ (Fig. 9A). Therefore, D is valid for the complete $S = 9/2$ spectrum, i.e. including both populations of rhombicity.

Next, we quantify the $S = 9/2$ spin concentration by double integration [26] of the subspectra from the $|\pm3/2>$ doublets. We take the $T = 12$ K spectrum in which the amplitude is maximally developed. The quantification of $S = 9/2$ spins gives a value of 0.6–1.3 prismane protein^{-1}. The uncertainty in this number depends on the uncertainties in D determination (±15%) and, especially, in the integration limits of partially resolved subspectra.

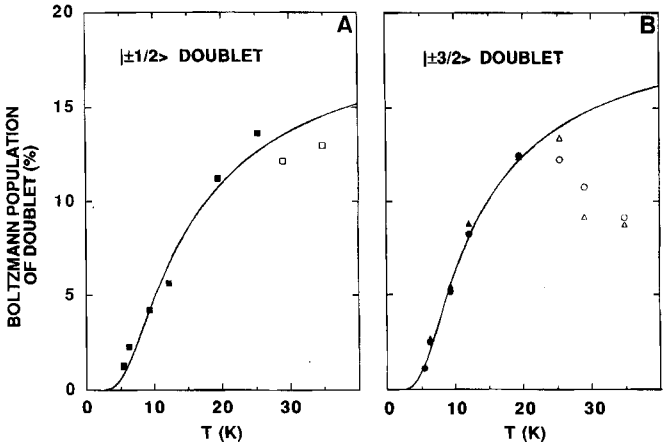

Fig. 9. Thermal (de)population of the highest doublet ($m_S = \pm1/2$) and the one-to-highest doublet ($m_S = \pm3/2$) of the inverted ($D < 0$) $S = 9/2$ multiplet in the prismane protein. The data points are the peak area at $g = 15.3$ (■), the amplitude at $g = 6.65$ (▲) and the area of the feature around $g \approx 5.5$ (●) multiplied by the detection temperature (i.e. corrected for Curie-law temperature dependence). The line plotted and the scaling of the ordinate were obtained by fitting the data to a Boltzmann distribution over the sublevels of an $S = 9/2$ system with $D = -0.86\ \text{cm}^{-1}$. The deviation above $T \approx 25$ K (○, □, △) reflects lifetime broadening.

Table 2. Frequency dependence of the $S = 9/2$ EPR. The zero crossing of the $g_{\text{eff}} \approx 5.5$ subspectrum in S-, X-, P- and Q-bands.

Microwave frequency	Zero crossing
GHz	g_{eff}
2.97	5.58
9.23	5.57
15.56	5.56
35.11	5.50

Frequency dependence and reduction potential of the $S = 9/2$ system

Effective g values of high-spin systems are a function of the microwave frequency. This dependency can in principle be used to determine D. We have attempted to measure the $S = 9/2$ spectrum at other than X-band frequencies. Due to the diminished sensitivity in these frequency bands, only the zero crossing of the $g \approx 5.5$ subspectrum was detected. The results are given in Table 2. Only a slight reduction in the effective g is observed with increasing frequency. This slight curvature is insufficient to determine D, however the data are not inconsistent with the previously determined $D = -0.86\ \text{cm}^{-1}$. Moreover, the data establish that the weak-field assumption ($S \cdot D \cdot S \gg g\beta B \cdot S$) is valid. We used this assumption in the calculation of g in Table 1.

The concentration of the $S = 9/2$ system is higher than the $S = 1/2$ signal of the $[6\text{Fe-}6\text{S}]^{5+}$ state by an order of magnitude. We hypothesize that the 5+ state is quantitatively accounted for by these two signals, i.e. 10% is $S = 1/2$ and 90% is $S = 9/2$. The situation bears analogy to that in the reduced Fe-protein of nitrogenase, for which we found 20% $S = 1/2$ and 80% $S = 3/2$ [27]. Morgan et al. later showed that these two spin systems in Fe-protein were indistinguishable biochemically, as their intensity ratio is a constant in redox

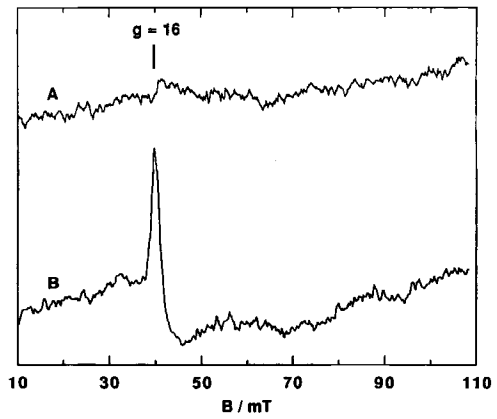

Fig. 10. Dual-mode spectrum of a low-field resonance from *D. vulgaris* prismane protein reduced with dithionite to the intermediate 4+ state. (A) Magnetic component of the microwave perpendicular to the external magnetic field vector; (B) the two vectors were parallel. EPR conditions, microwave frequencies, 9146 MHz (perpendicular) and 9098 MHz (parallel); microwave power, 200 mW; modulation amplitude, 1.25 mT; temperature, 9 K.

titrations [28]. Meyer and coworkers reached a similar conclusion on the basis of room temperature NMR [29]. We have performed a ratio-titration experiment on a concentrated sample of prismane protein. Starting from the isolated protein i.e. predominantly in the 5+ form, the prismane was titrated with small aliquots of Hepes-buffered dithionite. After each addition, the $S = 1/2$ and $S = 9/2$ EPR was measured. In multiple steps, the two signals were titrated away, resulting in the EPR silent $[6Fe\text{-}6S]^{4+}$ state. Throughout this titration, the intensity ratio $[S = 1/2]/[S = 9/2]$ was a constant within experimental error ($\pm 10\%$). The two spin systems are different magnetic ground states from the same biochemical entity with $E_m = +5$ mV at pH 7.5.

Parallel-mode, integer-spin EPR of the 4+ state

The 4+ state is silent in normal-mode EPR. The spin is expected to be integer or zero. Integer spin systems can have forbidden $|\Delta m_s| = 0$ transitions at low field. These transitions within non-Kramers doublets become allowed when the microwave magnetic component is configured parallel, rather than perpendicular, to the static magnetic field. The parallel-mode resonator provides this geometry, which has been proven practical in the EPR detection of $S = 2$ systems in metalloproteins [12].

In Fig. 10, low-temperature dual-mode spectra are presented from concentrated prismane protein in the 4+ state. We started from the isolated 5+ state and titrated with dithionite to the 4+ state, then to the 3+ state. In the isolated (5+) and in the fully reduced (3+) proteins, there is no parallel-mode signal, consistent with the detection of a quantitative $S = 1/2$ spectrum in normal-mode EPR. Contrarily, the 4+ state exhibits a relatively sharp, asymmetrically shaped feature at low field.

The asymmetric feature has its positive peak at $g \approx 16$ and its width is only a few millitesla. This spectrum is quite different from the $S = 2$ metalloprotein spectra previously reported: the spectra typically had a width of several tens of millitesla, and also had significant intensity in normal-mode EPR [12, 30, 31]. However, we also note a remarkable correspondence in that both the $S = 2$ spectra and the present Fig. 10B are asymmetric, single-line spectra. The $S = 2$ spectra were interpreted to come from the transition within the highest non-Kramers doublet with approximate g_{eff} of $4S \cdot g_{real}$, and this gives $g_{eff} \approx 8$ for $g_{real} \approx 2$. Extrapolating this model to the present case, we reach the tentative conclusion that $S = 4$.

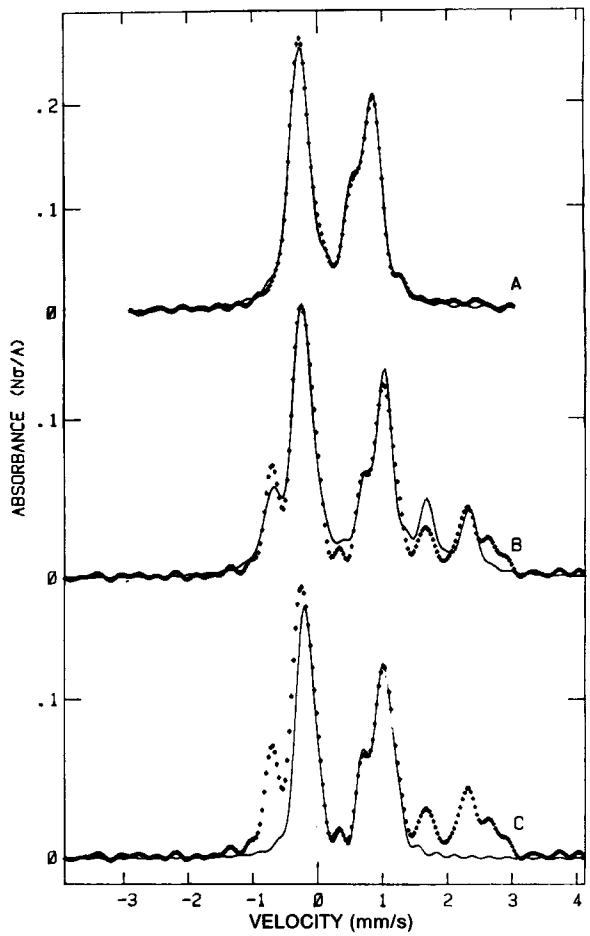

Fig. 11. High temperature, absorption mode, Mössbauer spectra and fits (——) for the prismane protein in the isolated (5+) and reduced states (3+). (A) Isolated protein, 125 K superimposed by a fit with two sites of occupancy 4 and 2 (see Table 3); (B) dithionite-reduced protein, 125 K superimposed by a four-site fit of occupancy 3, 1, 1 and 1; (C) same data as (B) superimposed by a two-site fit omitting the ferrous atoms.

Mössbauer spectroscopy of the 5+ and 3+ states

In Fig. 11 the absorption-mode, high-temperature Mössbauer spectra are shown for the dithionite-reduced form of the protein (the 3+ state) and for the isolated form of the protein (the 5+ state). These data are superimposed by computer simulations that model the spectra as sums of quadrupole pairs. The fitting parameters for these data as well as for those taken at 175 K (data not shown) are listed in Table 3. Quantitation of the spectra account for all the ^{57}Fe atoms in the samples. There are no resonances that are vanishingly small due to the presence of a large and anisotropic internal magnetic field in the atoms, because at these temperatures the magnetic moments from the paramagnetic electrons are averaged to Curie-Law values by the thermal processes. Therefore, the hyperfine fields in the $S = 1/2$ state in the reduced enzyme and the $S = 9/2$ state in the resting enzyme,

Table 3. A comparison of Mössbauer parameters for prismane and cubane models versus the prismane protein. The data for the model compounds were measured as part of the work described in [19, 32, 33]. For the protein data, the amount of iron is not a free parameter in the analysis, but is fixed by the high-temperature simulations and is identical for the high-field and low-field spectra (and agrees with the ICP-MS value). The Debye temperature for all irons in the protein is 160 K. Valency is the average of the formal valencies (i.e. ferric or ferrous) of all iron ions.

Sample	Valency	Temperature	Isomer shift	Quadrupole splitting	Line width	Occupancy (Fe atoms)
		K	mm/s			
$(Et_4N)_3Fe_6S_6(SR)_6$	2.5	125	0.44	1.04	–	6
$(Et_4N)_3Fe_6S_6(OR)_6$	2.5	125	0.48	1.03	–	6
$(Et_4N)_3Fe_6S_6I_6$	2.5	125	0.48	1.13	–	6
$(Et_4N)_3Fe_6S_6Br_6$	2.5	125	0.49	1.13	–	6
$(Et_4N)_3Fe_6S_6Cl_6$	2.5	125	0.50	1.10	–	6
$(Et_4N)_2Fe_6S_6Cl_6$	2.67	125	0.43	0.62	–	6
$(Et_4N)_2Fe_4S_4(SR)_4$	2.5	125	0.43	0.83	–	4
$(Et_4N)_2Fe_4S_4Cl_4$	2.5	125	0.49	1.04	–	4
This protein (3+)	2.5	125	0.52	1.27	0.27	3
			0.45	0.81	0.27	1
			0.80	2.02	0.27	1
			0.93	3.06	0.27	1
This protein (3+)	2.5	175	0.50	1.24	0.24	3
			0.41	0.79	0.24	1
			0.72	2.02	0.24	1
			0.90	3.03	0.24	1
This protein (5+)	2.83	125	0.40	1.18	0.28	4
			0.32	0.73	0.28	2
This protein (5+)	2.83	175	0.40	1.19	0.26	4
			0.33	0.71	0.26	2
This protein (5+)	2.83	4.2	0.44	1.16	0.28	4[a]
			0.36	0.7	1	1[b]
			0.36	0.7	1	1[c]

[a] Both computer simulations of the diamagnetic irons at this temperature have the same parameters ($\eta = 0$), except for the applied magnetic field.
[b] $A_x = A_y = A_z = -11$ mm/s, η is not determined, but is expected to be about 0.6.
[c] $A_x = A_y = A_z = -7.3$ mm/s, η is not determined, but is expected to be about 0.6.

which we know to be present due to our previous EPR experiments, are not factors in the Mössbauer spectra shown in Fig. 11. As a consequence, the charge parameters, isomer shift (δ) and quadrupole splitting (ΔE_q), are the only determinants of these spectra. In Table 3, the relevant parameters from a series of prismane model compounds in the 3− state are also shown. (The inorganic chemists count the exogenous iron ligands as part of the formal charge in the system. For cubanes, their charge is four less than that in the [4Fe-4S] cluster; for prismanes, their charge is six less than that in the [6Fe-6S] cluster.) The reduced form of the protein (3+) has the EPR signature of the 3− prismane model. Comparing the isomer shifts from the reduced-protein fit to those in Table 3, we see that four of the iron atoms match well (in Fig. 11C, the simulation has only these four iron sites), but an intensity that adds up to two iron equivalents is in a form suggestive of a formal high-spin ferrous atom such as that found in reduced rubredoxin or the reduced form of a [2Fe-2S] cluster. The mismatches in Fig. 11B for these ferrous sites indicate heterogeneity in the protein. Similar effects were reported above for the EPR of the 3+ state. Clearly, there is a difference between the cluster in this protein and that in a $Fe_6S_6(SR)_6$ cluster.

The $[4Fe\text{-}4S]^{2+}$ state and the $[6Fe\text{-}6S]^{3+}$ state are isoelectronic with very similar isomer shifts but unequal quadrupole splittings (Table 3). In both of these clusters, the appropriate interpretation of the formal charge for the irons is one of partial valence. The six iron atoms (three ferric and three ferrous) in a 3− prismane model give rise to a single quadrupole pair whose isomer shift changes by about +0.07 mm/s upon single-electron reduction (Table 3). Similarly the 2− cubane model has a single quadrupole pair whose isomer shift is slightly more sensitive to reduction than the prismane model. This added sensitivity to reduction is expected because the cubane has two less iron atoms/reducing electron than the prismane. The EPR-monitored redox titration has shown that there is a two-electron difference between the isolated and the dithionite-reduced forms of the protein. It is therefore possible that the two ferrous atoms, visible in the spectra from the dithionite-reduced enzyme but absent in those from the protein in the 5+ state, are the active redox center, while the other four iron atoms are part of a $[4Fe\text{-}4S]^{2+}$ cluster that is unchanged by this chemistry.

There are, however, several reasons to reject the possibility that a cubane is somehow involved with spectra in Fig. 11. Two of the iron atoms are in the high-spin ferrous state in the dithionite-reduced protein, therefore the other four iron atoms must be in the cubane if one exists. The isomer shift of these four irons agrees well with that of a $[4Fe\text{-}4S]^{2+}$ center, which is diamagnetic. Therefore, the $S = 1/2$, prismane-signature EPR spectrum would have to come from the two ferrous atoms; a very unlikely situation. In Fig. 12 the Mössbauer spectra of the dithionite-reduced protein in various temperatures and

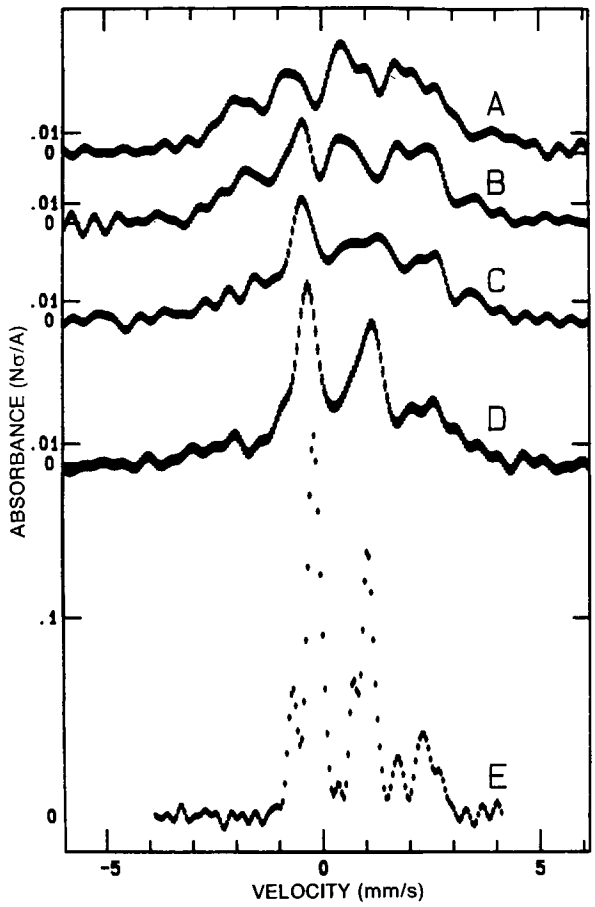

Fig. 12. Absorption-mode Mössbauer spectra of the dithionite-reduced prismane protein at various temperatures and applied magnetic fields. (A) 4.2 K, 5 T applied magnetic field; (B) 4.2 K, 30 mT; (C) 10 K, 30 mT; (D) 20 K, 30 mT; (E) 175 K, 0 mT.

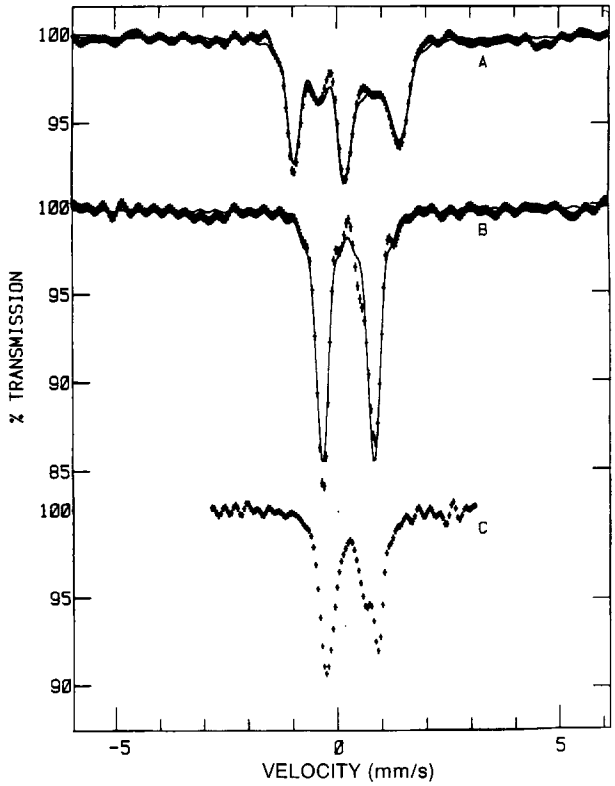

Fig. 13. Transmission-mode Mössbauer spectra and fits (——) of the isolated prismane protein (the 5+ state) at various temperatures and applied magnetic fields. (A) 4.2 K, 5 T applied magnetic field; (B) 4.2 K, 200 mT; (C) 175 K, 0 mT.

applied magnetic fields are shown. These spectra show that all six of the iron atoms are paramagnetic at low temperature, even at low applied fields. Therefore, all six iron atoms are part of one or more non-integer spin systems. The possibility of a $[4Fe\text{-}4S]^{2+}$ cluster is thereby excluded for this protein. Furthermore, the data in Fig. 12 also require the incorporation of the two ferrous atoms (Fig. 11) into the $S = 1/2$ state that quantitates to one electron equivalent by EPR. This conclusion necessitates a situation where the other four iron atoms have an odd number of electrons to account for the paramagnetism ($S = 1/2$ EPR) at low temperature.

In Fig. 13, the Mössbauer spectra for the isolated protein (5+) at various temperatures and magnetic fields are shown. These spectra have complexities that are not present in the data from the dithionite-reduced protein (Figs 11 and 12). For example, the spectra taken at high temperature (Figs 11A and 13C) fit well to a model with six iron atoms, where the simulations (Table 3) account for all the iron in the protein. However, at low temperature, four of the iron atoms (2/3 of the intensity of the spectra) fit well to a model that has a single-iron environment (Fig. 13A and B, Table 3). We interpret this finding to mean that four of the iron atoms are in a regular environment that appears to be nearly diamagnetic, even with the application of very high magnetic fields. The spectral shapes of the central lines in these spectra greatly resemble those of the dithionite-reduced spectra. However, they are shifted to smaller velocities (implying oxidation) by an amount that is greater than the shift characteristic of a single electron oxidation for either the prismanes or cubanes. However, at no temperature does one see the presence of the two ferrous irons that were so obvious in the dithionite-reduced protein. We interpret these data to signify that the two-electron difference between these two redox forms of the protein is accounted for by the oxidation of the two ferrous lines and the four-iron cluster. This can only be possible if the two ferrous irons and the four-iron cluster are part of a single cluster. Thus, we conclude that the spectra from both forms of the protein are characteristic of a six-iron cluster. This conclusion leads immediately to the problem of explaining the presence of an $S = 9/2$ signal for the six-iron cluster in the resting state of the protein, where four of the iron atoms have just been shown to be diamagnetic. The explanation of this apparent paradox lies in the wings of the spectra shown in Fig. 13A and B. Two of the iron atoms (1/3 total intensity) are almost invisible due to the presence of large internal magnetic fields. At 5 T applied magnetic field, the sizes of the induced magnetic fields along the non-easy axes (the perpendicular axes) for this ground state are nearly the size of the 'easy' axis (body-frame z-axis) fields. The electron Zeeman splittings at 5 T are such that the ground state changes its identity with the relative orientation of the protein in the magnetic field. In other words, the Zeeman splitting is sometimes larger than the zero-field splitting depending on field orientation. However, at all orientations the ground state has a large magnetic moment. Tentatively, we attribute the lack of electron-spin moment (and magnetic splitting in the Mössbauer spectrum) of four of the

irons to very small spin-projection operators ($S_1 \cdot S/S \cdot S$). It is also possible that this small moment is due to an asymmetric charge distribution over the six-iron cluster such that the spin density is very small over the four near-diamagnetic iron atoms. However, the latter hypothesis is hard to rationalize against the shape of Fig. 13C and the isomer-shift change for the four near-diamagnetic irons that accompanies chemical reduction of the protein (Table 3).

A spin coupling model for the $S = 9/2$ state

In its dithionite-reduced form, the protein has the EPR signal that is thought to be a signature for the 3+ prismane core. Four of the six-iron atoms in the protein mimic the Mössbauer properties of the thiol-prismane very well. Two of the iron atoms seem to be more ionic than those in the thiol-prismane. One structure that would have all of the spectroscopic properties of the protein would be a prismane where four of the six exogenous ligands are thiols and two are more ionic. These two ligands would be located at opposite ends of the prismane so that the other four irons are at geometrically equivalent positions as required by Fig. 13A. The most surprising aspect of this explanation for the spectroscopy is the apparent diamagnetism in the four irons at low temperature (Fig. 13A and B). On the other hand, it is perhaps more surprising that most cubanes and prismanes have demonstrated the property of distributed charge in having equal isomer shifts for their iron atoms while simultaneously demonstrating localized spin by giving large, non-equivalent internal fields. In this protein, we could be seeing for the first time a situation where the ground-state molecular-orbital averages both charge and spin over these four iron atoms.

The computer fit in Fig. 13A gave the best fit for an applied field that is 3% lower than the actual applied magnetic field. This discrepancy is almost an order of magnitude greater than our uncertainty in this measurement. Therefore, the diamagnetic four irons are not diamagnetic when inspected closely, but instead have an extremely low electron-magnetic moment. If we assume that the two high-spin ferrous atoms of the dithionite-reduced center are high-spin ferric atoms in the 5+ center, then it is possible to create an $S = 9/2$ total spin by coupling two $S = 5/2$ ferric atoms with an $S = 1/2$, 3/2 or 5/2 effective spin from the ground-state molecular orbital of the near-diamagnetic four iron atoms while maintaining the requirement that these irons have a very small magnetic moment (Fig. 14).

For all three possible combinations of spin vectors in Fig. 14, the ferric ($S = 5/2$) spin vectors have spin-projection operators close to 1/2. The sum of all spin-projection operators in any spin-coupling scheme is one. We have already hypothesized that the four diamagnetic irons have spin-projection operators near zero. Therefore, if the two ferric irons in the resting enzyme are high-spin ferric ions, they must have spin-projection operators near 1/2. In Fig. 14, we show a geometrical argument that forces the same conclusion. The geometrical diagram is quantum-mechanically rigorous under the assumptions given in the figure caption. If we further assume that the ionic iron atoms have A values near the ionic-bond limit, 2.2 mT/electron, then we can estimate the shape of their Mössbauer spectra at 4.2 K and 0.04 T applied magnetic field using the EPR data. (The EPR resonance field for the $g \approx 18$ signal at X-band is near 0.04 T.) At 4.2 K, 89% of the spin population is in the $|\pm 9/2>$ Kramers doublet with its g values approximately 0, 0 and 18 (Table 1). These g values describe a situation where the electronic spin moment, and

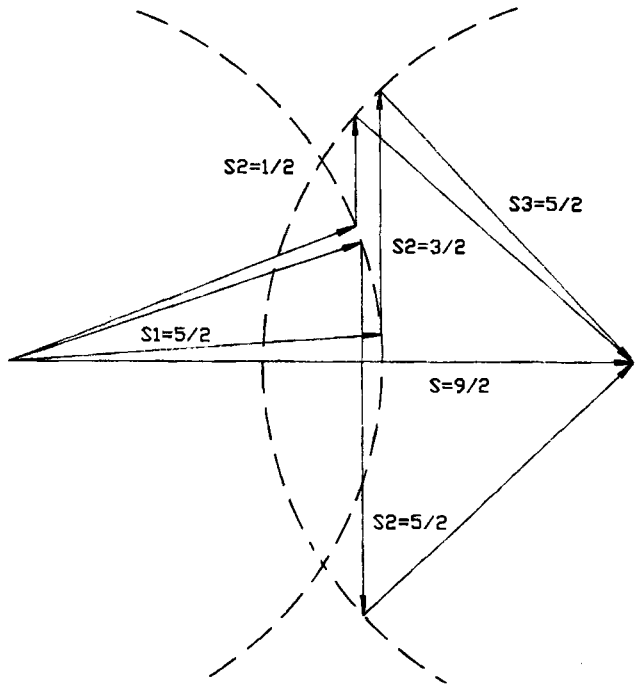

Fig. 14. Hypothetical spin-coupling schemes to obtain $S = 9/2$. The schemes show conservation of momentum constraints on a model where one high-spin ferric ion (S_1), one four-iron cluster (S_2) and one high-spin ferric ion (S_3) are coupled to form a resultant (S), where $S = 9/2$. The vectors are proportional to the magnitudes of the electron-spin moments assuming that the g values of all the components and the resultant are equal; therefore, $S = S_1 + S_2 + S_3$ describes a conservation of energy constraint as well as a type of coupling of angular momenta. S_2 is perpendicular to S, as required by the Mössbauer spectroscopic results. The schemes are drawn from two circles of radius equal to $\sqrt{(35/4)}$ (– – –) and vector of length $|S_2|$ drawn perpendicular to the resultant. The spin projection operators, $S_i \cdot S/S \cdot S$, for $i = 1, 2, 3$ for the three diagrams are for $S_2 = 1/2$, 0.55, 0.00, 0.45, for $S_2 = 3/2$, 0.59, 0.00, 0.41, and for $S_2 = 5/2$, 0.56, 0.00, 0.44.

therefore the nuclear spin moment, are precessing around the z-axis of a coordinate system fixed with respect to the protein regardless of the orientation of the 0.04-T applied magnetic field. The Mössbauer spectrum is six lines of intensity: 3:2:1:1:2:3. With the above assumptions, the internal field at the ferric irons should be 50 T and give a six-line pattern with a 16-mm/s range.

On the other hand, the Mössbauer spectrum of the two ferric atoms has some complexities above the simple explanation given above. A high-spin ferric atom usually has a magnetic hyperfine interaction that is large (negative) and isotropic and a quadrupole spectrum that is small and rhombic, therefore the nuclear Hamiltonian would seem to be dominated by the magnetic interaction and therefore be a simple pattern. In fact, the electronic Hamiltonian for the $|\pm 9/2>$ Kramers doublet cannot be separated from the nuclear Hamiltonian at low applied magnetic fields. Simulations show that, as the applied magnetic field is increased from the Earth's magnetic field (0.06 mT in our laboratory) to a few tenths of a millitesla, the Mössbauer spectrum changes from an asymmetric four-line pattern to a very symmetric six-line pattern. The g tensor has diagonal values of 0, 0 and 18 (assuming that the $g \approx 18$ signal corresponds to the body-frame z-axis), therefore the electron Zeeman interaction for

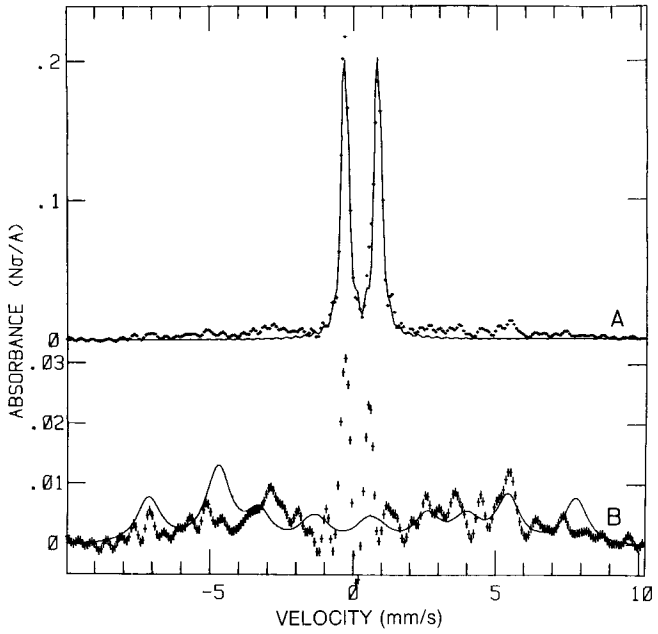

Fig. 15. Low temperature, low-applied-magnetic-field spectra of the isolated prismane protein. (A) The experimental data at 4.2 K and 0.04 T applied magnetic field superimposed (——) by a single-site model for the four diamagnetic irons (parameters in Table 3); (B) the difference of the spectra in (A) superimposed by the simulation of the two ferric sites (parameters in Table 3). Note the importance of our data reduction methods to the quantitation of these spectra.

various powder orientations is non-zero only to the extent that the body-frame z-axis is along the applied field. When the applied field component along the body-frame z-axis is larger than 2 mT, then the Hamiltonian is so dominated by the electronic terms that only the nuclear terms along this z-axis have an appreciable effect on the spectrum. An example of these effects is given in Appendix. For the orientations where the electronic terms are dominant, the spectra are six-line patterns where only A_z and V_{zz} alter the spectra significantly.

If the applied magnetic field is 0.04 T, then the electronic terms dominate the Hamiltonian in 99% of the body orientations. At 4.2 K, the maximum electronic Zeeman splitting is 0.3 cm^{-1}, so one can ignore the effects of Boltzmann populations at this field other than to realize that 89% of the spin systems are in the $|\pm 9/2>$ Kramers doublet. One should therefore expect a superimposition of two six-line patterns to account for the experimental spectra, with the spectra from the other Kramers doublets making small contributions. Fig. 15B shows the difference spectrum obtained after the subtraction of the diamagnetic four iron atoms previously discussed (Fig. 15A). These four irons are not quite perfectly modelled by the single environment shown in Table 3; therefore, there are two spikes in the center of the spectrum. The difference spectrum has almost exactly the area of two iron equivalents as does the simulation (parameters in Table 3). The simulation has two iron environments, both with large negative A (−11 and −7.3 mm/s) and both with small isomer shifts (0.2 mm/s) and small quadrupole splittings (0.7 mm/s) as expected for high-spin ferric ions. The A difference can be attributed to a difference in the sites, seen in the quadrupole pairs of the ferrous irons in the reduced protein, or to difference in the spin-projection operators. There is no way to separate these

Table 4. Calculated internal magnetic fields (A values) for various spin-coupling models.

S_2	S_1	S_3
	T (mm/s)	
1/2	−42 (−9.9)	−34 (−8.0)
3/2	−45 (−10.7)	−31 (−7.3)
5/2	−43 (−10.2)	−34 (−8.0)

effects experimentally. By scaling the ionic-limit A values to form a best fit to the measured values, we calculate the A values in Table 4 (S_2 denotes the spin from four diamagnetic iron atoms). The fit for $S_2 = 3/2$ is exact, but possibly fortuitous because A values for high spin ferric ions in biology can easily vary by 10%.

The computer simulation in Fig. 15 also necessitated an extremely large line width. The only parameter that seems capable of generating this kind of line-width broadening is V_{zz}, therefore we have concluded that either the quadrupole splitting (unlikely) or the direction of the g tensor relative to the quadrupole tensor is distributed for this spin system in the as isolated (5+) protein. We have seen heterogeneity in the Mössbauer (Fig. 11B) and EPR (Fig. 1B) spectra of the reduced protein. This may carry over to the as isolated 5+ state, as indicated by the observation of two rhombicities in the $S = 9/2$ EPR. We have not attempted to include heterogeneity in the simulation of Fig. 15. With the above qualifications, we claim that the fit in Fig. 15B accounts for the last two irons in the sample, proves the origin of the coupling to form the $S = 9/2$ multiplet and is an example of a new and unique type of Mössbauer spectrum: that of a widely anisotropic electronic spin system in a weak applied magnetic field.

Concluding remarks

In Results and Discussion, we have presented an explanation for many of the spectroscopic properties of the putative prismane protein at least with respect to EPR and Mössbauer spectroscopies. We now review our conclusions to emphasize their contraints on possible structures for the novel metal cluster of this protein. The emerging picture is a six-iron cluster, where two of the iron atoms are charge-localized (similar to those in a [2Fe-2S] cluster) and four are similar to those in a [6Fe-6S] prismane model cluster. The redox chemistry of the novel cluster is centered about the two ionic irons, but also involves the other four irons. The spin coupling in the 5+ state gives rise to an $S = 9/2$ ground state with the $|\pm 9/2>$ doublet lowest at low applied magnetic fields. This coupling depends on a ferromagnetic coupling of the two ionic iron atoms. Accordingly, these iron atoms are expected to be separated by the other four-iron atoms to allow the ferromagnetic coupling. A mixed-ligand prismane, where the ionic irons are at opposite ends of the prismane with exogenous hard Lewis-base ligands (nitrogen or oxygen), has these properties. It is an attractive possibility to identify these ligands with the nitrogen ligation that was implicated by multi-frequency EPR from the $S = 1/2$ minor species with all values of $g < 2$. However, any other arrangement compatible with the above constraints would be equally valid.

The unusually high system spin $S = 9/2$ has thus far been tentatively identified in three iron-sulfur enzymes: dis-

similatory sulfite reductase [6], carbon-monoxide dehydrogenase [8] and the FeMo-protein of nitrogenase [5]. Several synthetic iron cluster compounds with $S = 9/2$ ground states have also recently been described [34–36]. However, in these models the bridging is $(\mu\text{-OR})_2$ or $(\mu\text{-OH})_3$. Also, their Mössbauer properties are quite distinct from those of the $S = 9/2$ system reported here [35, 36]. Very recently, an Fe/S-protein from *D. desulfuricans* (ATCC 27774), with hydrodynamic and EPR properties comparable to our *D. vulgaris* prismane protein (this paper) [5, 9, 11]), has been briefly described [37]. It is presently not clear how (dis)similar the two proteins are: the Mössbauer data, the redox properties and the metal analysis of the *D. desulfuricans* protein [37] appear to be rather different from those presented here.

We propose that the *D. vulgaris* monomeric prismane protein is a suitable model for the complex iron-sulfur redox enzymes, not only because it carries an iron-sulfur supercluster with associated superspin, but also because this cluster is capable of accepting more than one reducing equivalent within a physiologically relevant potential range. Our ongoing research efforts are presently focussed at obtaining primary and tertiary structural information on this remarkable protein.

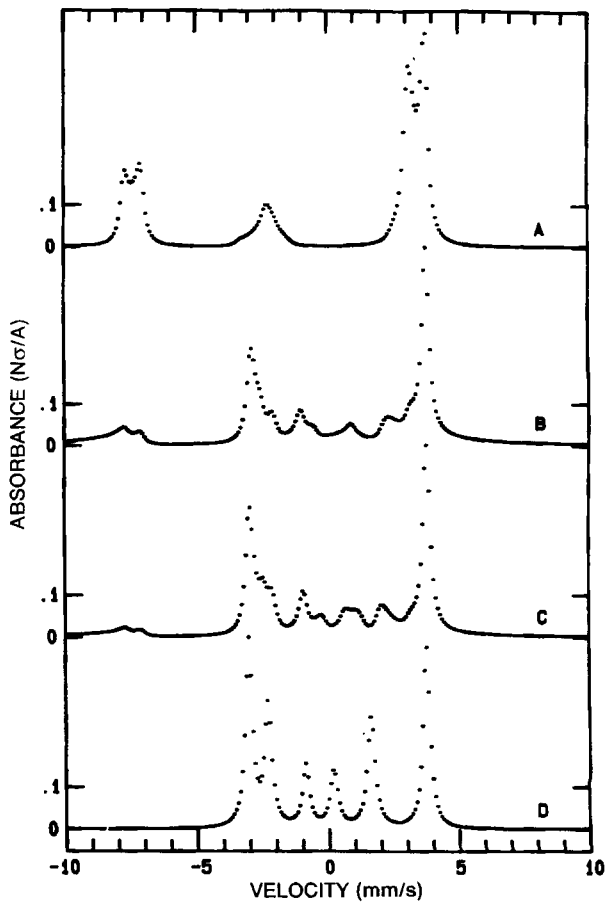

Fig. 16. Computer synthesized spectra of an $S = 9/2$ system at different but small applied magnetic fields. With $\Delta E_q = 0.7$ mm/s, $\eta = 0$ and $A_x = A_y = A_z = -5$ mm/s, the spectra show the effect of an increasing magnetic field. The applied field is 0 (A), 0.5 mT (B), 1 mT (C) and 40 mT (D).

APPENDIX

To initiate the calculation, we assume that the zero-field Hamiltonian, $H = D_e[S_z^2 - S(S+1)/3] + E_e(S_x^2 - S_y^2)$, has created the zero-order situation where the electronic ground state is an $m_S = \pm 9/2$ Kramers doublet. It is also assumed that this is the only occupied electronic state and that coupling to all other states can be ignored. The assumptions are consistent with the measured value of $D_e \approx -0.86\ \text{cm}^{-1}$ by EPR. The Kramers doublet has $g \approx 0$, 0 and 18 (for an effective spin one-half), indicating that the electronic spin is precessing around the z-axis of the body-frame exclusively. The Hamiltonian for the combined electronic nuclear transitions is

$$H = g\beta_e B_{app} \cdot \cos\Theta \cdot m_s + A_{xx}I_xS_x + A_{yy}I_yS_y + A_{zz}I_zS_z + 2DI_z^2 + (E-D)I_x^2 + (-E-D)I_y^2, \quad \text{(A1)}$$

where $\Delta E_q = 6D(1+\eta^2/3)$, $E = \eta D$, and Θ is the angle between the applied field, B_{app}, and the z-axis of the body coordinate system. If we write the Hamiltonian in the product basis set, $|m_I m_S>$, then the nuclear ground state ($I = 1/2$) matrix is

	$\|+1/2, +1/2>$	$\|+1/2, -1/2>$	$\|-1/2, +1/2>$	$\|-1/2, -1/2>$
$< +1/2, +1/2 \|$	$A_z/4 + \alpha/2$	0	0	$A_x/4 - A_y/4$
$< +1/2, -1/2 \|$	0	$-A_z/4 - \alpha/2$	$A_x/4 + A_y/4$	0
$< -1/2, +1/2 \|$	0	$A_x/4 + A_y/4$	$-A_z/4 + \alpha/2$	0
$< -1/2, -1/2 \|$	$A_x/4 - A_y/4$	0	0	$A_z/4 - \alpha/2$

(A2)

where $\alpha = g\beta_e B_{app} \cdot \cos\Theta$. The corresponding matrix can be solved trigonometrically as

$$E_{1,2} = -(A_z/4) \pm (\alpha/2)\cos(2\Theta_1) \mp [(A_x + A_y)/4]\sin(2\Theta_1),$$
$$\Psi_1 = -\sin\Theta_1 \,|+1/2, -1/2> + \cos\Theta_1 \,|-1/2, +1/2>,$$
$$\Psi_2 = +\cos\Theta_1 \,|+1/2, -1/2> + \sin\Theta_1 \,|-1/2, +1/2>, \quad \text{(A3)}$$

where $\tan(2\theta_1) = (A_x + A_y)/(-2\alpha)$, and

$$E_{3,4} = (A_z/4) \pm (\alpha/2)\cos(2\Theta_2) \pm [(A_x - A_y)/4]\cos(2\Theta_2),$$
$$\Psi_3 = +\cos\Theta_2 \,|+1/2, +1/2> + \sin\Theta_2 \,|-1/2, -1/2>,$$
$$\Psi_4 = -\sin\Theta_2 \,|+1/2, +1/2> + \cos\Theta_2 \,|-1/2, -1/2>, \quad \text{(A4)}$$

where $\tan(2\Theta_2) = (A_x - A_y)(2\alpha)$.

The excited nuclear state ($I = 3/2$) forms an 8×8 matrix with the effective $S = 1/2$ spin system. This matrix blocks into two 4×4 matrices as follows:

	$\lvert +3/2, +1/2 \rangle$	$\lvert +1/2, -1/2 \rangle$	$\lvert -1/2, +1/2 \rangle$	$\lvert -3/2, -1/2 \rangle$
$< +3/2, +1/2 \rvert$	$3A_z/4 + 3D + \alpha/2$	$\sqrt{3}(A_x - A_y)/4$	$\sqrt{3}E$	0
$< +1/2, -1/2 \rvert$	$\sqrt{3}(A_x - A_y)/4$	$-A_z/4 - 3D - \alpha/2$	$(A_x + A_y)/2$	$\sqrt{3}E$
$< -1/2, +1/2 \rvert$	$\sqrt{3}E$	$(A_x + A_y)/2$	$-A_z/4 - 3D + \alpha/2$	$\sqrt{3}(A_x - A_y)/4$
$< -3/2, -1/2 \rvert$	0	$\sqrt{3}E$	$\sqrt{3}(A_x - A_y)/4$	$3A_z/4 + 3D - \alpha/2$

(A5)

and

	$\lvert +3/2, -1/2 \rangle$	$\lvert +1/2, -1/2 \rangle$	$\lvert -1/2, -1/2 \rangle$	$\lvert -3/2, +1/2 \rangle$
$< +3/2, -1/2 \rvert$	$3A_z/4 + 3D - \alpha/2$	$\sqrt{3}(A_x - A_y)/4$	$\sqrt{3}E$	0
$< +1/2, +1/2 \rvert$	$\sqrt{3}(A_x - A_y)/4$	$-A_z/4 - 3D + \alpha/2$	$(A_x + A_y)/2$	$\sqrt{3}E$
$< -1/2, -1/2 \rvert$	$\sqrt{3}E$	$(A_x + A_y)/2$	$-A_z/4 - 3D - \alpha/2$	$\sqrt{3}(A_x - A_y)/4$
$< -3/2, +1/2 \rvert$	0	$\sqrt{3}E$	$\sqrt{3}(A_x - A_y)/4$	$3A_z/4 + 3D + \alpha/2$

(A6)

Transition intensities are calculated as in Kundig [38] except that $\Delta m_S = 0$ and the transition dipole operator can be integrated over its azimuth angle (the angle around the propagation vector), but it cannot be integrated over its polar angle because the terms in the Hamiltonian matrices that contain α are not independent of this angle. They depend on $\Theta(\alpha = g\beta_e B_{app} \cdot \cos\Theta)$, which happens to be equal to the polar angle because the propagation vector of the radiation field is parallel to the applied-magnetic-field direction. Therefore, the transition intensities containing I_+ and I_- have a factor $(1 + \cos^2 \Theta)/2$ while the intensities containing I_z have a factor $\sin^2 \Theta$. The integration over the angle, Θ, is performed explicitly by incrementing $\cos \Theta$ as described in [39]. An example of the output of this program for increasing values of the applied magnetic field is shown in Fig. 16. When only the Earth's magnetic field is present on the sample (Fig. 16A), the spectrum exemplifies the situation where the nuclear and electronic spins are coupled to form a resultant. This situation is common in paramagnetic proteins [23]. When the electron Zeeman term is much greater than the magnetic hyperfine term (Fig. 16D), the spectrum exemplifies those with a strong magnetic field oriented in body frame [38]. This situation is much different from that encountered in most paramagnetic proteins where the internal magnetic field is oriented along the applied magnetic field.

In the case described here the direction of the internal field (spatial quantization) is determined completely by the zero-field splitting term in creating the effective g tensor with only one non-zero component in its principal-axis (diagonal) representation. It is important to realize that this kind of spatial quantization is usually overlooked by theoreticians because of Kramers theorem: there is a degeneracy in half-integer spin systems (time reversal symmetry) that cannot be removed by zero-field splitting terms. The proof of Kramers theorem seems to prevent spatial quantization. However, we believe that the kind of spatial quantization described here can be generalized to lattice structures, providing both the very large g values and the magnetic anisotropy necessary as a basis for the understanding of hard and soft ferromagnetism.

We are grateful to R. B. G. Wolbert for help in preparing the proteins used in this work. We thank Professor C. Veeger for his continuing interest and support. Dr. S. P. J. Albracht has kindly provided us access to the parallel-mode and multi-frequency EPR facility at the Department of Biochemistry, The University of Amsterdam. We thank Drs C. Hess-Riechmann and K. Schneider at the University of Bielefeld for the ICP-MS determinations. The iron-sulfur model compounds, referred to in Table 4, were prepared by Professor D. Coucouvanis and his collaborators at The University of Michigan. This investigation was supported by the Netherlands Foundation for Chemical Research (SON) with financial aid from the Netherlands Organization for Scientific Research (NWO) and by the National Institutes of Health (Grant GM-32785 to RHS).

REFERENCES

1. Hagen, W. R., van Berkel-Arts, A., Krüse-Wolters, K. M., Dunham, W. R. & Veeger, C. (1986) *FEBS Lett. 201*, 158–162.
2. Hagen, W. R., van Berkel-Arts, A., Krüse-Wolters, K. M., Voordouw, G. & Veeger, C. (1986) *FEBS Lett. 203*, 59–63.
3. Voordouw, G., Hagen, W. R., Krüse-Wolters, K. M., van Berkel-Arts, A. & Veeger, C. (1987) *Eur. J. Biochem. 162*, 31–36.
4. Hagen, W. R., Wassink, H., Eady, R. R., Smith, B. E. & Haaker, H. (1987) *Eur. J. Biochem. 169*, 457–465.
5. Hagen, W. R., Pierik, A. J., Wolbert, R. B. G., Wassink, H., Haaker, H., Veeger, C., Jetten, M. S. M., Stams, A. J. M. & Zehnder, A. J. B. (1991) *J. Inorg. Biochem. 43*, 237.
6. Pierik, A. J. & Hagen, W. R. (1991) *Eur. J. Biochem. 195*, 505–515.
7. Jetten, M. S. M., Hagen, W. R., Pierik, A. J., Stams, A. J. M. & Zehnder, A. J. B. (1991) *Eur. J. Biochem. 195*, 385–395.
8. Jetten, M. S. M., Pierik, A. J. & Hagen, W. R. (1991) *Eur. J. Biochem. 202*, 1291–1297.
9. Hagen, W. R., Pierik, A. J. & Veeger, C. (1990) *Ital. Biochem. Soc. Trans. 1*, 85.
10. Pierik, A. J., Wolbert, R. B. G., Mutsaers, P. H. A., Hagen, W. R. & Veeger, C. (1992) *Eur. J. Biochem. 206*, 697–704.
11. Hagen, W. R., Pierik, A. J. & Veeger, C. (1989) *J. Chem. Soc. Faraday Trans. 1 85*, 4083–4090.
12. Hagen, W. R. (1982) *Biochim. Biophys. Acta 708*, 82–98.
13. Albracht, S. P. J. (1973) *J. Magn. Reson. 13*, 299–303.
14. Stevenson, R. C. (1982) *Triplet state EPR: an application to three iron-sulfur flavoproteins*, Ph. D. thesis, The University of Michigan.
15. Dunham, W. R., Wu, C. T., Polichar, R. M., Sands, R. H. & Harding, L. J. (1977) *Nucl. Instrum. Methods 145*, 537–553.

16. Filter, W. F. (1983) *High-resolution* ^{57}Fe Mössbauer spectroscopy, Ph. D. thesis, The University of Michigan.
17. Dunham, W. R., Hagen, W. R., Braaksma, A., Grande, H. J. & Haaker, H. (1985) *Eur. J. Biochem. 146*, 497–501.
18. Dunham, W. R., Carroll, R. T., Thompson, J. F., Sands, R. H. & Funk, M. O. (1990) *Eur. J. Biochem. 190*, 611–617.
19. Kanatzidis, M. G., Hagen, W. R., Dunham, W. R., Lester, R. K. & Coucouvanis, D. (1985) *J. Am. Chem. Soc. 107*, 953–961.
20. Hagen, W. R. (1989) in *Advanced EPR; applications in biology and biochemistry* (Hoff, A. J., ed.), pp. 785–812, Elsevier, Amsterdam.
21. Dunham, W. R., Fee, J. A., Harding, L. J. & Grande, H. J. (1980) *J. Magn. Reson. 40*, 351–359.
22. Tsibris, J. C. M., Tsai, R. L., Gunsalus, I. C., Orme-Johnson, W. H., Hansen, R. E. & Beinert, H. (1968) *Proc. Natl Acad. Sci. USA 59*, 959–965.
23. Sands, R. H. & Dunham, W. R. (1975) *Quart. Rev. Biophys. 7*, 443–504.
24. Anderson, R. E., Anger, G., Petersson, L., Ehrenberg, A., Cammack, R., Hall, D. O., Mullinger, R. & Rao, K. K. (1975) *Biochim. Biophys. Acta 376*, 63–71.
25. Hagen, W. R. & Albracht, S. P. J. (1982) *Biochim. Biophys. Acta 702*, 61–71.
26. Aasa, R. & Vänngård, T. (1975) *J. Magn. Reson. 19*, 308–315.
27. Hagen, W. R., Eady, R. R., Dunham, W. R. & Haaker, H. (1985) *FEBS Lett. 189*, 250–254.
28. Morgan, T. V., Prince, R. C. & Mortenson, L. E. (1986) *FEBS Lett. 206*, 4–6.
29. Meyer, J., Gaillard, J. & Moulis, J.-M. (1988) *Biochemistry 27*, 6150–6156.
30. Hagen, W. R., Dunham, W. R., Sands, R. H., Shaw, R. W. & Beinert, H. (1984) *Biochim. Biophys. Acta 765*, 399–402.
31. Hagen, W. R., Dunham, W. R., Johnson, M. K. & Fee, J. A. (1985) *Biochim. Biophys. Acta 828*, 369–374.
32. Kanatzidis, M. G., Dunham, W. R., Hagen, W. R. & Coucouvanis, D. (1984) *J. Chem. Soc. Chem. Commun. 1984*, 356–358.
33. Coucouvanis, D., Kanatzidis, M. G., Dunham, W. R. & Hagen, W. R. (1984) *J. Am. Chem. Soc. 106*, 7998–7999.
34. Snyder, B. S., Patterson, G. S., Abrahamson, A. J. & Holm, R. H. (1989) *J. Am. Chem. Soc. 111*, 5214–5223.
35. Surerus, K. K., Münck, E., Snyder, B. S. & Holm, R. H. (1989) *J. Am. Chem. Soc. 111*, 5501–5502.
36. Ding, X.-Q., Bominaar, E. L., Bill, E., Winkler, H. & Trautwein, A. X. (1990) *J. Chem. Phys. 92*, 178–186.
37. Ravi, N., Moura, I., Tavares, P., LeGall, J., Huynh, B. H. & Moura, J. J. G. (1991) *J. Inorg. Biochem. 43*, 252.
38. Kundig, W. (1967) *Nucl. Instrum. Methods 48*, 219–228.
39. Hagen, W. R., Hearshen, D. O., Harding, L. J. & Dunham, W. R. (1985) *J. Magn. Reson. 61*, 233–244.